Eur. Phys. J. B **52**, 507–519 (2006)
DOI: 10.1140/epjb/e2006-00329-0

THE EUROPEAN PHYSICAL JOURNAL B

Behavior of a wetting phase near a solid boundary: vapor near a weakly attractive surface

A. Oleinikova, I. Brovchenko[a], and A. Geiger

Physical Chemistry, Dortmund University, 44221 Dortmund, Germany

Received 22 December 2005 / Received in final form 29 May 2006
Published online 21 August 2006 –

Abstract. Density profiles of a LJ vapor near a weakly attractive surface with long-range fluid wall potential was studied along the pore coexistence curve. There are two localized density maxima near the pore wall: the first one is caused by localization of the molecules in the minimum of the fluid-wall potential, and the second one reflects adsorption of molecules at the first layer at higher densities. In addition, a third, weak density maximum is observed close to the critical temperature due to the competition between the long-range attractive tail of the fluid-wall potential and the effect of missing neighbors. This maximum separates the region of a gradual density depletion toward the surface due to the missing neighbor effect and the adsorption region further from the surface, where the density gradually increases toward the surface due to the attractive fluid-wall potential. When approaching the bulk critical temperature, this maximum moves away from the surface due to the divergence of the bulk correlation length. Applicability of various equations to describe the vapor density profiles is examined. Excess adsorption of vapor at low temperatures turns into excess depletion at higher temperatures. The crossover temperature increases with increasing pore size and strengthening fluid-wall interaction. The problems of the theory of the surface critical behavior of Ising models in a case of a non vanishing surface field and its mapping on a fluid is discussed.

PACS. 05.70.Jk Critical point phenomena – 05.70.Np Interface and surface thermodynamics – 64.70.Fx Liquid-vapor transitions – 68.43.-h Chemisorption/physisorption: adsorbates on surfaces

1 Introduction

A fluid near a solid boundary becomes inhomogeneous and its various properties differ essentially from the bulk case. Knowledge of a spatial fluid density distribution is necessary to characterize the local structural and dynamic properties of inhomogeneous fluid. Besides, this is important for understanding the phenomena directly related to fluid inhomogeneity, such as attraction between extended solvophobic surfaces, slipping flow, adsorption in porous media, etc. Search for the laws which are able to predict density distribution near various solid boundaries at various thermodynamic conditions is therefore important challenge for physics of fluids. These laws should account for the location of the thermodynamic state point of a fluid in respect to the liquid-vapor phase transition and its critical point.

Near a smooth surface, inhomogeneity of a fluid may be characterized by the local density profile $\rho(z)$, where z is the distance to the surface. The local density distribution is determined by the competition of two effects, which are caused by a solid wall. The first effect is caused by the unavoidable weakening of the potential energy of molecules due to the lower number of nearest neighbors of fluid molecules near the wall (the so-called effect of missing neighbors). This is the single effect of the solid boundary in the simplest cases of a hard-wall or free boundary conditions. The second effect of the surface is related to the attractive interaction U_w between the fluid molecules and a solid wall. The theory of fluids near a boundary is based on the minimization of the grand potential Ω (Helmholtz free energy) of the inhomogeneous fluid, providing an equality of the chemical potential everywhere in the system [1]. The equilibrium density distribution satisfies

$$\frac{\partial \Omega}{\partial \rho(r)} = 0. \tag{1}$$

A fruitful approach to solve this problem is the density functional theory, where the free energy is considered as an unique functional of the density distribution [2]. In this case the equilibrium distribution of the local density is a solution of an integro-differential equation, which, however, can not be solved analytically even for simple geometries. Therefore, the equilibrium density profiles in all

[a] e-mail: alla@pc2a.chemie.uni-dortmund.de

modifications of the density functional theory can be obtained only numerically. Note, that the intrinsic mean-field character of density functional theories limits their ability to reproduce fluid properties when approaching the critical point, where long-range correlations become important.

Alternatively, equilibrium density profiles of fluids can be obtained from computer simulations. Such computer experiment can provide valuable data even near the critical point, when the effect of the finite size of the simulation system is taken into account properly [3]. Even sophisticated experimental techniques can provide only an approximate description of the fluid density distribution near a solid boundary (see, for example, Refs. [4–7]). Therefore, computer simulations remain currently the main source of "experimental" data, which can be used to test available theories and/or to develop empirical equations able to predict the density profile near any boundary at any thermodynamic state.

The theory of the critical phenomena provides an exact and highly universal description of the thermodynamic properties of a bulk fluid in proximity of the critical point [8,9]. For some of these properties, such as the temperature dependence of the densities along the liquid-vapor coexistence curve, the critical contribution remains dominant even far away from the critical point [10,11]. Similar to bulk systems, the theory of the surface critical behavior in Ising magnets provides a highly universal description of the systems near the boundary [12]. Recently, it was shown how the behavior of a confined fluid can be mapped on the surface critical behavior of Ising magnets [10,11,13,14]. Such a mapping should provide scaling equations for the density profiles in various thermodynamic states. In particular, the *order parameter* profiles $\Delta\rho(z,\tau)$ (difference between the local densities $\rho_l(z,\tau)$ and $\rho_v(z,\tau)$ of the coexisting liquid and vapor phases) near a weakly attractive surface can be mapped on the surface universality class of an *ordinary* transition. The order parameter profiles in a wide range of temperatures, starting from the vicinity of the critical point, can be describe by a universal exponential equation, which contains only two bulk properties: density and correlation length.

A surface phase transition (wetting or drying) [15] influences the density profile in one of the coexisting phases only. This essentially complicates the fluid density profile in that phase, which undergoes surface transition. An attractive long-range fluid-wall interaction suppresses a drying transition up to the critical temperature. In this case a drying (not vapor) layer develops in the liquid phase near the wall with increasing temperature [16]. This drying layer is strongly sensitive to the confinement and can almost completely vanish in small pores [10,14]. Note, that the liquid density profile can be described in a universal way even in the presence of a drying layer [16]. In the present paper we study the density profile of a *wetting* phase, which does not undergo a surface phase transition, namely vapor near a weakly attractive wall.

It is reasonable to map density profiles of a *wetting* phase (as well as of a supercritical fluid) onto magnetization profiles of semiinfinite Ising magnets. In the case of a free surface (surface field $h_1 = 0$), the magnetization profile *m(z)* is flat and equal to zero at $T \geq T_c$. In the case of a strong (infinite) surface field ($h_1 \to \infty$), the missing neighbor effect can be neglected and the short-distance behavior of magnetization follows the power law [17]:

$$m(z) \sim z^{-\frac{\beta}{\nu}}. \tag{2}$$

where $\nu \approx 0.63$ and $\beta \approx 0.326$ are the bulk critical exponents [18]. So, *increase* of magnetization toward the surface is governed by the exponent $-\beta/\nu \approx -0.52$ for the 3D Ising model. At $T = T_c$ when the bulk correlation length $\xi = \infty$, the power law (2) should describe a complete density profile. At $T \geq T_c$, equation (2) is valid for distances $z \ll \xi$, whereas for $z \gg \xi$ the local magnetization *m(z)* approaches the value of the bulk magnetization $m_b = 0$ exponentially:

$$m(z) - m_b \sim e^{-z/\xi}. \tag{3}$$

Various empirical equations, which incorporate both long-distance and short-distance behaviors were proposed for $T > T_c$ (see [19–21]).

If the surface field is not very strong, a non-monotonous magnetization profile should be expected [22,23]. The missing neighbor effect yields a steep *decrease* of the magnetization toward the surface and the short-distance behavior of magnetization $T \geq T_c$ should be [23]:

$$m(z) \sim z^k, \tag{4}$$

where $k \approx 0.21$. When moving away from the surface, the increase of *m(z)* described by equation (4) is expected up to the distance z_{max}, where the switch to the magnetization decay, described by equation (2) occurs. The value z_{max} should increase with vanishing surface field and can extend up to a distance larger than ξ [24]. In the case of such a weak surface field, the dependence (2) is not observed. It is important, that in case of a weak surface field, a new relevant length scale z_{max} appears in addition to the correlation length and pore size.

The magnetization profiles at subcritical temperatures $T \leq T_c$ were much less studied. It was established, that in the case of a zero surface field ($h_1 = 0$) in both coexisting phases the magnetization decreases when approaching the surface and at short distances *m(z)* should obey a power law [17,25]:

$$m(z) \sim z^{\frac{\beta_1-\beta}{\nu}}, \tag{5}$$

where and $\beta_1 \approx 0.82$ [26] is the surface critical exponent, which describes the temperature dependence of the order parameter below the critical temperature T_c [12]. Thus, the *decrease* of magnetization toward the surface, which is caused solely by the *missing neighbor effect*, should be governed by the exponent $(\beta_1 - \beta)/\nu \approx 0.78$. At distances larger than ξ, the local magnetization increases and approaches the bulk magnetization exponentially (Eq. (3)).

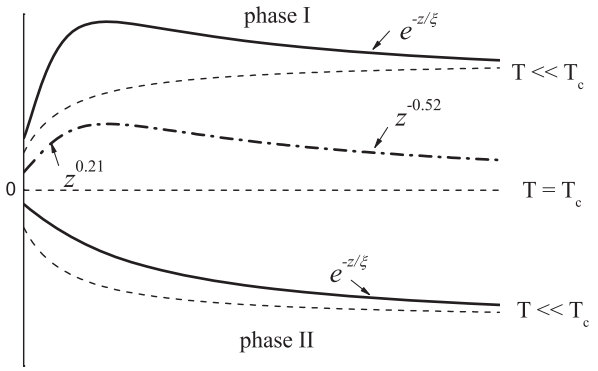

Fig. 1. Sketch of the magnetization profiles *m(z)* of an Ising magnet near a boundary at $T = T_c$ and at $T \ll T_c$. Zero surface field $h_1 = 0$: dashed lines. Non-zero surface field $h_1 \neq 0$ attracting upward spins: solid and dot-dashed lines.

In the case of a strong surface field, a similar shape of the magnetization profiles below and above the critical temperature was predicted [20,21]. This theory takes into account a response to the surface field (quite similar above and below T_c), but neglects *spontaneous* magnetization below T_c near the surface [10,14]. Therefore, the theory given in references [20,21] could not be applied for finite surface fields at $T < T_c$.

The magnetization profiles in two coexisting phases below T_c in the presence of a weak surface field have not been studied yet even at the mean-field level. General arguments allow to expect a nonmonotonous magnetization profile not only above but also below the critical temperature. At subcritical temperatures, which exceed the wetting temperature there is a single magnetization profile of the wetting phase, since only one of the phases (wetting phase) remains near the surface. Very close to T_c, it should look like *m(z)* at $T = T_c$ (dot-dashed line in Fig. 1), however, with an exponential decay of magnetization at large distances. Below the wetting transition temperature there are two local magnetization profiles near the surface for any surface field (dashed and solid lines in Fig. 1). A maximum of *m(z)* can be expected in the wetting phase, where the missing neighbor effect and the surface field favor opposite trends of *m(z)* near the surface. This maximum separates the region, where the magnetization decreases steeply toward the surface due to effect of missing neighbors, and the "adsorption" region far from the surface, where magnetization gradually increases toward the surface due to the surface field.

Mapping of the magnetization profiles of Ising magnets onto the density profiles in fluids is not obvious, as even mapping of the surface critical behavior and the order parameter of the phase transition near the surface in these systems is an area of debates [10,14]. Additional complications arise from the long-range fluid-wall attraction, which is typical for real systems. Studies of the fluid density profiles near various surfaces along the liquid-vapor phase transition line and in the supercritical region should clarify these questions.

Recently, a maximum of the density profiles of a one component fluid was reported for $T = T_c$ [27]. In this paper a zero surface field in an Ising model was assumed to be equivalent to some nonzero value of an attractive fluid-wall potential, corresponding to the so-called 'neutral wall'. Such a mapping, however, does not explain the monotonous depletion of the density toward the surface, when the fluid-wall potential is weaker than the "neutral wall" value. Note, that such asymmetry seems to be absent in binary mixtures at the liquid-liquid critical point [29].

In the present paper we study the density profiles *ρ(z)* in the vapor phase of a LJ fluid along the pore coexistence curve from the freezing to the critical temperature. Near a weakly attractive surface, liquid phase undergoes a drying transition and density profiles are distorted by the presence of a drying layer [16]. Saturated vapor near a weakly attractive surface is a "wetting" phase and does not undergo the surface phase transition. We have tested the ability of the theory of the surface critical behavior to describe evolution of the vapor density profile along the liquid-vapor coexistence curve. For completeness, the density profiles in various regimes far from the critical point are characterized. The effects of the confinement and the fluid-wall interaction potential on the vapor density profiles are discussed.

2 Simulated systems

We studied the Lenard-Jones (LJ) fluid, having an interparticle interactions of the form:

$$U_{LJ}(r) = 4\epsilon \left[(\sigma/r)^{12} - (\sigma/r)^{6} \right], \qquad (6)$$

where ϵ measures the well depth of the potential, while σ sets the length scale. The potential was spherically truncated at a radius 2.5σ and left unshifted. No long-range corrections were applied to account for effects of the truncation. The density ρ used in the present paper is the number density scaled by σ^3, while T is the temperature scaled by ϵ/k_B, where k_B is Boltzmann's constant. Liquid and vapor densities of this fluid at the bulk coexistence curve from freezing temperature to the critical temperature were obtained in our previous paper [10].

To study the behavior of the two coexisting phases near a surface, the LJ fluid was confined in a slitlike pore with structureless walls. Each wall interacts with the particles of the fluid via a long-range potential comprising a single plane of LJ molecules:

$$U_w(z) = 4\epsilon\ f\ \left[0.4\,(\sigma/z)^{10} - (\sigma/z)^{4} \right], \qquad (7)$$

where z measures the distance to the wall and the parameter f determines the strength of the fluid-wall interaction. No truncation was applied to $U_w(z)$. In the present paper we report mainly the results obtained for a weakly attractive (solvophobic) surface with a well-depth of the

fluid-wall interaction $U_{w1}(z) = U_w(z, f = 0.3)$, which provides about 70% of the well-depth of the fluid-fluid interaction. This surface is "strongly solvophobic" and simple estimation [28] gives a contact angle of about 145° for a liquid phase at low temperatures. To explore the effect of the strength of the fluid-wall potential on the vapor density profile we also simulated the liquid-vapor coexistence in a pore with slightly stronger fluid-surface interaction $U_{w2}(z) = U_w(z, f = 0.4)$. Additionally, the effect of the range of the fluid-wall interaction was explored by simulation of a system with a slower decay of the fluid-wall potential $U_{w3}(z)$, which follows from the integration over all interactions with LJ molecules in a half-space and can be described by the equation:

$$U_{w3}(z) = 4\epsilon f^* \left[(\sigma^*/z)^9 - (\sigma^*/z)^3 \right]. \quad (8)$$

The parameters of the potential $U_{w3}(z)$ were adjusted to get equal well depths at equal distances of the potentials $U_{w3}(z)$ and $U_{w1}(z)$. This was achieved using $\sigma^* = 0.8328\sigma$ and $f^* = 0.468$ in equation (8).

The distance z in equation (7) is not a fully appropriate measure of the distance of molecules to the surface, since part of this distance is not accessible for molecules. As a result, the first minimum of the fluid density profiles, which indicates the border between the first and second surface layer, is located noticeably away from $z = 1\sigma$. A more reasonable measure of the distance of molecules to the surface was introduced in [10,14,16]. Since the fluid-wall interaction described by equation (7) is equal to zero at the distance 0.86σ from the pore wall, it is reasonable to divide this interval equally between the volumes of the fluid and the solid. However, the distance of about 0.55σ near the pore wall, in fact, is not accessible for the centers of fluid molecules. Therefore, $\Delta z = z - 0.55\sigma$ we consider as the most appropriate definition of the distance between the center of a molecule and the pore wall.

To approach a semi-infinite surface geometry, we reduce the influence of the confinement on the vapor density profiles $\rho_v(\Delta z, \tau)$ by simulations of the liquid-vapor coexistence in very large pore of width $H = 40\sigma$. To study the effect of pore size on $\rho_v(\Delta z,\tau)$, we also simulated the liquid-vapor coexistence in a small pore of width $H = 12\sigma$.

3 Methods

The properties of a vapor near a weakly attractive surface were studied along the pore coexistence curve, i.e. in equilibrium with the liquid phase. The coexistence curve of the confined LJ fluid was determined using Monte Carlo simulations in the Gibbs ensemble (GEMC) [30]. GEMC simulations allow to achieve direct equilibration of two coexisting phases, which are simulated at a given temperature simultaneously in two simulation cells. Equality of the pressures in the coexisting phases is achieved by random changes of the volumes of the simulation boxes, keeping the total volume of the two boxes constant. Equality of the chemical potentials in the two phases is achieved by molecular transfers between the simulation boxes. Efficient molecular transfers [31] enable to obtain highly accurate values of the coexisting densities in a wide temperature range from freezing temperature to the pore critical temperature. For each temperature point the number of successful transfers between the coexisting phases varied from dozens per particle at the lowest temperatures to several hundreds near the pore critical temperature.

The total number of molecules in the liquid and vapor phases in the large pore of width $H = 40\sigma$ in the GEMC simulations was about 8000. The average lateral size L of the simulation box which contains the vapor phase was about 20σ. The number of molecules in the vapor phase N_v varied from ∼100 at the lowest studied temperature to ∼4000 when approaching the critical temperature. More details of the simulations, parameters of the model fluid, as well as its bulk coexistence curve and the coexistence curve in a small pore of width $H = 12\sigma$ are given in our previous papers [10,16].

The densities of the coexisting phases were obtained at 28 temperatures (from $T = 0.75$ to $T = 1.60$) in the pore with $H = 40\sigma$ and at 26 temperatures (from $T = 0.60$ to $T = 1.30$) in the pore with $H = 12\sigma$. The lowest studied temperatures were close to (or even below) the bulk triple-point temperature of a LJ fluid (values from 0.687 to 0.692 were reported in the literature [32–34]). The highest studied temperatures ($T = 1.13$ and 1.16) were slightly below the pore critical temperatures estimated as $T_c = 1.145$ [10] and $T_c = 1.165$ [16], for the small and large pore, respectively. The bulk coexistence curve obtained in [10] by GEMC simulations was found to be consistent with the bulk critical temperature $T_c = 1.1876$ obtained using a histogram reweighting method with subsequent mixed-field finite size scaling [35]. The reduced temperature used in the present paper $\tau = 1 - T/T_c$ measures the deviation of the temperature from the *bulk* critical temperature.

The density profiles of the vapor were obtained by Monte Carlo (MC) simulations in the NVT ensemble, using the average densities of the vapor phase obtained in the GEMC simulations and approximately the same number of molecules in the simulation box. The strong density gradient near the pore wall and the large pore width makes the determination of reliable density profiles in such pores very time consuming. This problem was overcome by using two kinds of moves in MC simulations in the NVT ensemble. The first kind of moves is a standard MC move with a maximal displacement of a molecule, which provides an acceptance probability of about 50%. The second kind of move is a long-distance molecular transfer inside the simulation box: an attempt to place randomly chosen fluid molecule into a randomly chosen position. This move is similar to the one used in GEMC simulations for molecular transfers between the two simulation boxes. Such long-distance molecular transfers essentially improve the sampling of density profiles. The local density was determined for layers of 0.02σ width. The resulting density profiles were averaged over 10^5 configurations, taken each 1000th MC step. This yielded a statistical uncertainty of the local density $\rho(z)$ of less than 1%.

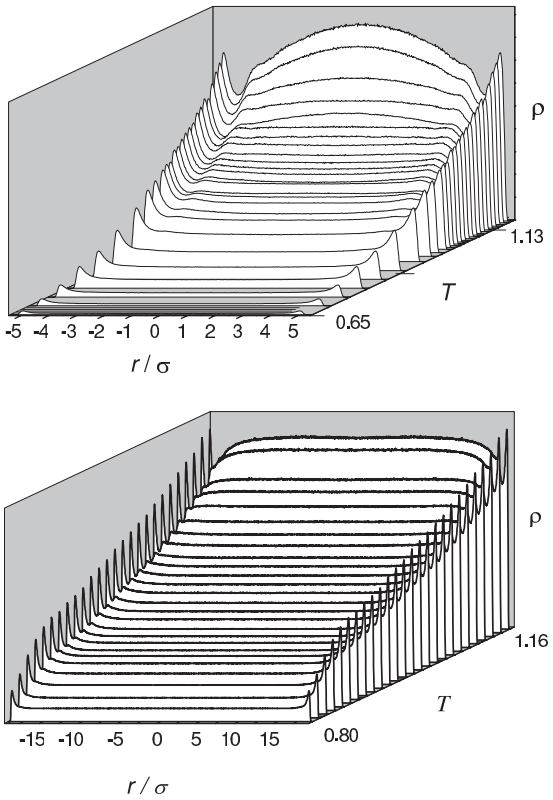

Fig. 2. Temperature evolution of the density profiles in the vapor phases along the coexistence curves of the LJ fluid confined in slitlike pore with $H = 12\sigma$ (upper panel) and $H = 40\sigma$ (lower panel). r is the distance to the pore center.

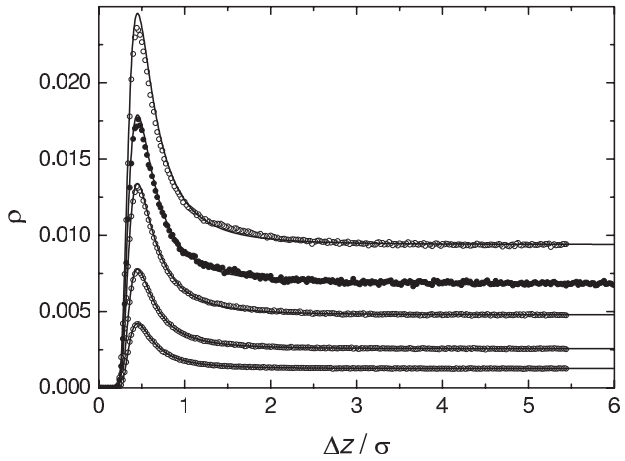

Fig. 3. Density profiles of saturated LJ vapor in a pore with $H = 12\sigma$ at $T = 0.6$, 0.65, 0.7 and 0.75 (open circles). Data at $T = 0.75$ for pore $H = 40\sigma$ are shown by solid circles. Boltzmann equation (9) with ρ_b equal to the density in the pore center is shown by solid lines.

4 Results

4.1 Adsorption of low-density vapor

The simulated density profiles of vapor along the pore coexistence curve for small and large pores are shown in Figure 2. The maximum of the vapor density near the wall is pronounced in the whole temperature range and increases with temperature similarly in both pores. Close to the triple point temperature, the vapor density profiles can be perfectly described by the Boltzmann formula for the density distribution of ideal gas in an external field:

$$\rho(\Delta z, \tau) = \rho_b \exp\left(-\beta^* U_w(z)\right), \tag{9}$$

where ρ_b is the vapor density far from the surface, β^* is the inverse product of temperature and Boltzmann constant k_B. For the fluid-wall interaction potential used in the present paper (Eq. (7)), the Boltzmann formula (9) reads:

$$\rho(\Delta z, \tau) = \rho_b \exp\left[-4f\left(0.4\left(\sigma/z\right)^{10} - \left(\sigma/z\right)^4\right)/T\right]. \tag{10}$$

The vapor density profiles in small and large pores and equation (10) are shown in Figure 3 for several temperatures close to the triple point. Evidently, the maximum of $\rho_v(\Delta z, \tau)$ corresponds to the minimum of the fluid-wall potential.

The location of the *first* density maximum coincides in the vapor and liquid [10,11,16] phases in the whole range of the liquid-vapor coexistence. So, in the considered temperature and density ranges, this maximum originates exclusively from the location of the fluid molecules in the well-depth of the *fluid-wall* interaction potential. Only in extremely dense fluids the repulsion between the fluid molecules slightly shifts this maximum toward the surface [10]. Localization of the fluid molecules in the first layer creates an effective "surface" potential for the other fluid molecules with a well-depth, located about 1σ from the first layer. This effect causes oscillations of the local fluid density, which decay on moving away from the surface. In the liquid phase several oscillations can be observed at low temperatures, whereas in the saturated LJ vapor only two density oscillations can be detected.

When the density of the saturated vapor exceeds 0.02 (at $T > 0.80$), an ideal-gas approach *overestimates* the adsorption of the vapor at the surface (see Fig. 4, solid lines). When intermolecular interactions are not negligible, the isothermal compressibility χ of the real gas becomes larger than the one of the ideal gas and the response of the fluid to the surface field may be expected to be stronger in accordance with the following equation [36,37]:

$$\rho(\Delta z) = \rho_b \exp\left[-U_w(z)\rho_b\chi\right]. \tag{11}$$

The isothermal compressibility χ of the homogeneous fluid at low densities may be presented by a virial expansion

$$\rho_b\chi/\beta^* = 1 - 2B(T)\rho_b - 3C(T)\rho_b^2 + ..., \tag{12}$$

where *B(T)* and *C(T)* are the second and third virial coefficient, respectively. The second virial coefficient for the interaction potentials, which decay faster than r^{-3} at large r, may be calculated by equation:

$$B(T) = -2\pi \int \left[\exp\left(-\beta U_{LJ}\right) - 1\right] r^2 dr. \tag{13}$$

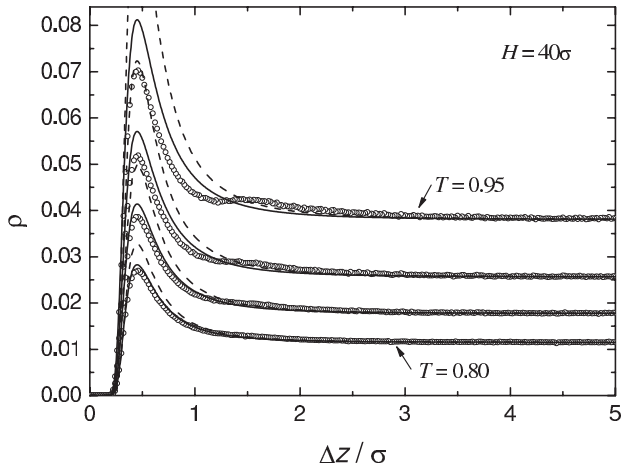

Fig. 4. Density profiles of saturated LJ vapor in a pore with $H = 40\sigma$ at $T = 0.8$, 0.85, 0.9 and 0.95 (open circles). Boltzmann equation (9) and equation (11) with ρ_b equal to the density in the pore center are shown by solid and dashed lines, respectively.

For the truncated LJ interaction potential used in the present simulations, the integral in equation (13) should have an upper limit 2.5σ. The second virial coefficient calculated at various temperatures with equation (13) are given in Table 1. The density profiles calculated by equations (11) and (12), truncated at the second virial coefficient, are shown in Figure 4 by dashed lines. As it was noticed before [36,37], equation (11) essentially overestimates the fluid adsorption near a pore wall and deviates from the real density profiles even more than the Boltzmann approach (9).

Overestimation of the adsorption calculated with equations (9) and (11) originates from neglecting the missing neighbor effect, which causes weakening of the potential energy of the molecules near the boundary due to the absence of fluid molecules on the other side of boundary. Indeed, when deriving equation (11), the reference homogeneous system (in the absence of a surface field) was assumed as a continuous fluid without boundary [36,37]. Note, that in (9) the missing neighbor effect is absent intrinsically. Weakening of the fluid-fluid interaction energy U_{LJ}^{av} per molecules near the surface causes a depletion of density and this effect is proportional to the value of U_{LJ}^{av} in the bulk fluid. That is why the missing neighbor effect should be taken into account always when U_{LJ}^{av} is not negligible. Note also, that both the ideal gas approach (Eq. (9)) and the rare gas approach (Eq. (11)) are not able to reproduce the second density oscillation, which becomes noticeable at $T \geq 0.90$ (see Fig. 4).

4.2 Crossover from adsorption to depletion

Although the second oscillation is still visible up to the pore critical temperature (see Fig. 2), the vapor density profiles at $\Delta z > 2$ remain practically smooth in the whole studied temperature and density range. In particular, the gradual adsorption of the fluid spreads deeper into the pore interior with increasing temperature and at $T = 1.08$ to 1.10 it is visible over 6 to 8σ from the surface (see Fig. 5). The surface perturbations, such as the missing neighbor effect and the short-range surface field, decay exponentially with an increasing distance from the surface and this decay is governed by the bulk correlation length [12,17]. This exponential behavior may be distorted by the long-range fluid-wall potential. However, we still may expect an exponential decay of the surface perturbations when the fluid-wall interaction is weak. In this case, the smooth part of the density profiles may be described by the following empirical equation:

$$\rho(\Delta z) = \rho_b + (\rho_s - \rho_b) \exp\left(-\frac{\Delta z}{\xi_-^{eff}}\right), \qquad (14)$$

where ρ_s is an effective surface density at $\Delta z = 0$ and ξ_-^{eff} is the effective correlation length, which describes

Table 1. The values ρ_b of the vapor density in the center of the pore with $H = 40\sigma$ at various temperatures T (reduced temperatures τ). The second virial coefficient $B(T)$, calculated with equation (13), and the dimensionless isothermal compressibility $\rho_b\chi/\beta^*$, calculated with equation (12). The ratio of ρ_b to the density of ρ_b^0 of the saturated bulk vapor.

T	τ	ρ_b $\pm 0.1\%$	$B(T)/\sigma^3$	$\rho_b\chi/\beta^*$	ρ_b/ρ_b^0
0.75	0.368	0.00685	–8.02	1.110	1.373
0.80	0.326	0.01149	–7.14	1.165	1.171
0.85	0.284	0.01775	–6.40	1.228	1.091
0.90	0.242	0.02565	–5.78	1.297	1.036
0.93	0.217	0.03250	–5.45	1.354	1.047
0.95	0.200	0.03807	–5.24	1.398	1.062
0.96	0.192	0.0413	–5.14	1.423	1.075
0.97	0.183	0.0430	–5.05	1.432	1.044
0.98	0.175	0.0463	–4.95	1.456	1.050
0.99	0.166	0.0489	–4.86	1.473	1.037
1.00	0.158	0.0521	–4.77	1.494	1.033
1.01	0.150	0.0572	–4.69	1.532	1.061
1.02	0.141	0.0611	–4.60	1.557	1.061
1.03	0.133	0.0654	–4.52	1.585	1.062
1.04	0.124	0.0708	–4.44	1.621	1.077
1.05	0.116	0.0750	–4.36	1.645	1.068
1.06	0.107	0.0795	–4.29	1.672	1.059
1.07	0.099	0.0846	–4.21	1.701	1.054
1.08	0.091	0.0889	–4.14	1.724	1.037
1.09	0.082	0.0961	–4.07	1.767	1.045
1.10	0.074	0.1027	–4.00	1.804	1.041
1.11	0.065	0.1106	–3.94	1.851	1.043
1.12	0.057	0.1208	–3.87	1.910	1.057
1.13	0.049	0.1305	–3.81	1.965	1.056
1.14	0.040	0.1380	–3.74	1.999	1.028
1.15	0.032	0.1606	–3.68	2.137	1.094
1.155	0.027	0.1643	–3.65	2.152	1.066
1.16	0.023	0.1685	–3.62	2.170	1.039

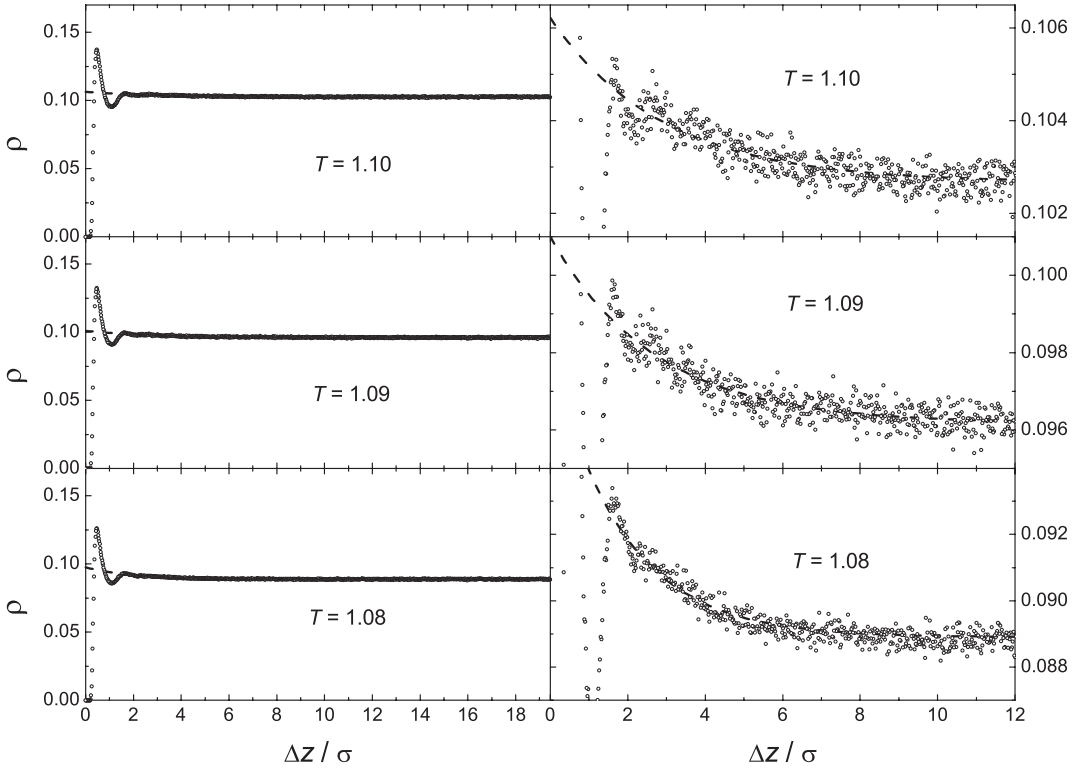

Fig. 5. Density profiles of saturated LJ vapor in a pore with $H = 40\sigma$ are shown by open circles in normal and enlarged scales in the left and right panels, respectively. Fits to equation (14) in the range $\Delta z \geq 2\sigma$ are shown by dashed lines.

intrusion of the surface perturbation into the bulk fluid. The fits of equation (14) to the smooth part of the density profiles ($\Delta z \geq 2\sigma$) are shown in Figure 5. The values of the fitting parameter ξ_-^{eff} and their error bars, which represent 95% confidence intervals, are shown in Table 2. The surface density ρ_s approaches the bulk density with increasing temperature. For example, ρ_s/ρ_b=1.097 at $T =$ 1.08 and $\rho_s/\rho_b = 1.034$ at $T = 1.10$. When $\rho_s > \rho_b$, the value of ξ_-^{eff} exceeds the bulk correlation length ξ_- estimated from the analysis of the order parameter profiles [10] and liquid density profiles [16] (see Tab. 2 and Fig. 6). Obviously, this reflects the slower decay of the surface perturbation caused by long-range tail of fluid-wall potential in comparison with exponential decay governed by the bulk correlation length. The difference between ξ_-^{eff} and ξ_- increases when the density profile becomes almost flat ($\rho_s \approx \rho_b$ at $T \approx 1.115$), i.e. when the missing neighbor effect and the surface field roughly compensate each other.

When the temperature increases to $T = 1.11$, a clear maximum can be seen in the density profile at $\Delta z_{max} \approx 3\sigma$ (see Fig. 7, open circles). The nature of this maximum can not be related to density oscillations due to the attraction of molecules to the second layer, as a minimum and not a maximum should appear at $\Delta z = 3\sigma$ in such a case. This density maximum is also clearly seen at $T = 1.12$ and 1.13 and its position moves away rapidly from the surface with increasing temperature. At higher temperatures, the density maximum is much weaker, but still visible in large scale. Its position Δz_{max} is shown by arrows in Figures 7 and 8 and also given in Table 2.

Table 2. Location Δz_{max} of the maximum of the density profiles in vapor and liquid phases, obtained directly from simulations and from equation (26). The values of the parameter ξ_-^{eff} and their standard deviations were determined from the fits of the vapor density profiles to equation (14). The values of the bulk correlation length ξ_- were obtained from the analysis of the liquid density profiles [16].

T	Vapor			Liquid	
	Δz_{max} sim.	Δz_{max} Eq. (26)	ξ_-^{eff} Eq. (14)	Δz_{max} sim.	ξ_- Ref. [16]
1.02	–	–	1.24 ± 0.03	7	0.82
1.03	–	–	1.31 ± 0.03	10	0.89
1.04	–	–	1.35 ± 0.03	7	0.87
1.05	–	–	1.47 ± 0.03	10	0.95
1.06	–	–	1.60 ± 0.04	10	1.10
1.08	–	–	1.86 ± 0.05	9.	1.16
1.09	–	–	2.69 ± 0.11	9.5	1.31
1.10	–	–	2.91 ± 0.14	11	1.47
1.11	3	3.45	3.93 ± 0.44	11	1.57
1.12	4.5	4.55	0.31 ± 0.03	11.5	1.68
1.13	6	5.8	0.79 ± 0.03	13	1.95
1.14	7.5	7.5	0.97 ± 0.02	16	2.14
1.15	9.5	9.7	1.70 ± 0.02	18	2.40
1.155	–	11.3	1.86 ± 0.03	16	2.91
1.16	12	13.5	1.90 ± 0.02	–	3.32

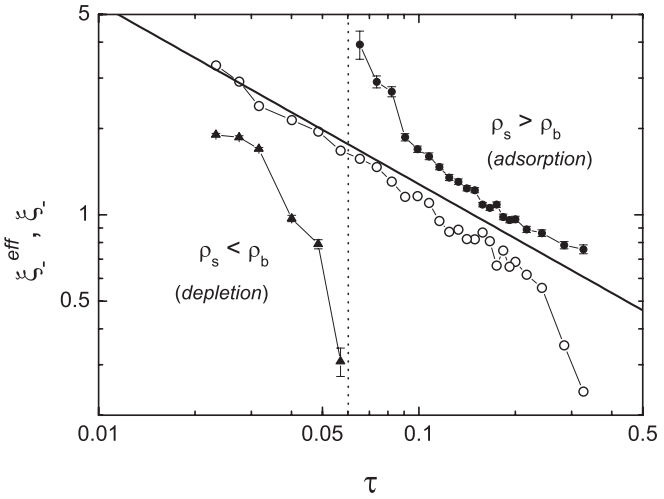

Fig. 6. Temperature dependence of the effective correlation length ξ_-^{eff} determined from the fits of the vapor density profiles to equation (14): $T < 1.115$ (solid circles), $T > 1.115$ (solid triangles). $T = 1.115$ is shown by vertical dotted line. Correlation length ξ_- determined from the liquid phase [16] is shown by open circles. The solid line represents the asymptotic power law $\xi_- = 0.30\ \sigma\tau^{-\nu}$ determined from the order parameter in small pore [10].

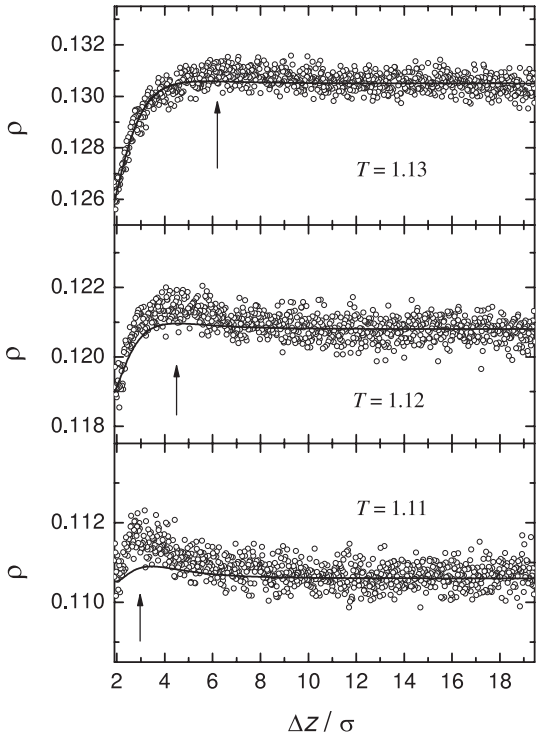

Fig. 7. Density profiles of a saturated LJ vapor in a pore with $H = 40\sigma$ are shown by open circles in enlarged scales. Equation (26) for respective temperatures is shown by solid lines. Maxima of density profiles located at Δz_{max} are indicated by arrows.

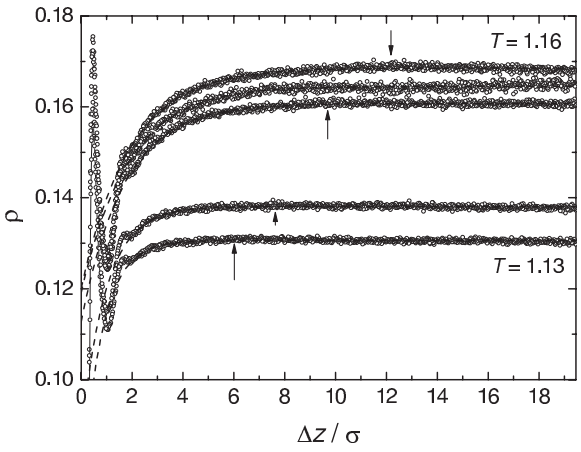

Fig. 8. Density profiles of the saturated LJ vapor in the pore with $H = 40\sigma$ at $T = 1.13$, 1.14, 1.15, 1.155 and 1.16 are shown by open circles in enlarged scale. Fits by the exponential equation (14) are shown by dashed lines. Maxima of the density profiles located at Δz_{max} are indicated by arrows.

4.3 Depletion of high-density vapor

At high temperatures close to the bulk critical temperature, the profiles of the vapor apart from the first two layers near the surface are convex upwards and $\rho_v(\Delta z,\tau)$ can be described by the equation (14) with $\rho_s < \rho_b$. The fits of the vapor density profiles by the equation (14) are shown by dashed lines in Figure 8 for the 5 highest temperatures studied. Evidently, the exponential equation (14) provides a good description of the depletion of the vapor in the range $\Delta z \geq 2\sigma$. The values of ξ_-^{eff} obtained from the fits (Tab. 2) are noticeably smaller than the bulk correlation lengths ξ_- [10,16]. This should be attributed to the long-range fluid-wall potential, whose effect is opposite to the general density depletion dominating at high temperatures. The discrepancy between ξ_-^{eff} and ξ_- is maximal when T is close to 1.115, where the density profile is almost flat and decreases when approaching the pore critical temperature (Tab. 2, Fig. 6). Note, that the deviation of the correlation length from the asymptotic temperature dependence is different in the bulk liquid and vapor phases, whose asymmetry strongly enhances when moving away from the critical temperature.

4.4 Interplay between density depletion and long-range attraction

The maximum of the density profile of a vapor phase is observed at temperatures $T \geq 1.11$ (see arrows in Figs. 7, 8 and Tab. 2). In the density profiles of the coexisting liquid phase a maximum of the density profiles was also detected (see Fig. 5 (inset) in Ref. [16] for $T = 1.10$). In the liquid phase this maximum can be seen at $T \geq 1.02$. An example of a liquid density profile with a maximum is shown in Figure 8 for the temperature $T = 1.04$. Although the amplitude of a maximum is very small (upper panel) it can be clearly seen in large scale (lower panel). The locations Δz_{max} of the maximum in the density profiles of the liquid are shown in Table 2 and in Figure 10. In both phases

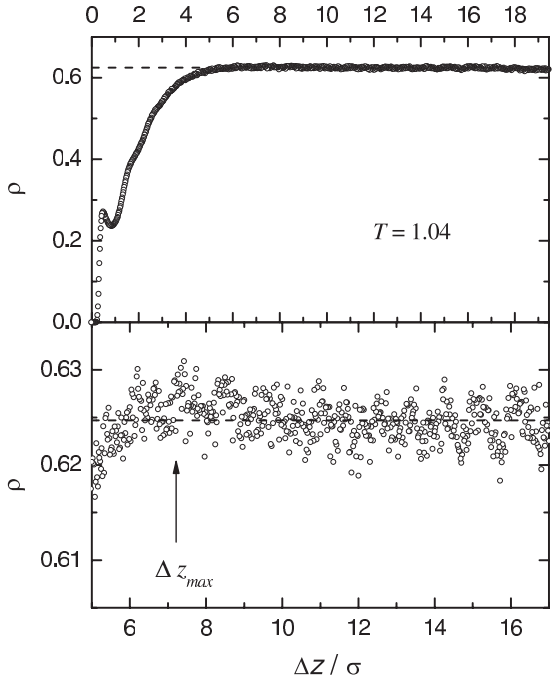

Fig. 9. Density profile of the saturated LJ *liquid* in the pore with $H = 40\sigma$ at $T = 1.04$ in normal (upper panel) and enlarged (lower panel) scales is shown by open circles. Density in the pore center $\rho_b = 0.6247$ is shown by a dashed line. The maximum of the density profile, located at Δz_{max}, is indicated by arrow.

the density maximum moves away from the surface with increasing temperature. The temperature dependence of Δz_{max} in the vapor phase shows almost perfect logarithmic behavior and can be described by the equation

$$\Delta z_{max}(\sigma) = -8.58 \ln \tau - 20.2, \tag{15}$$

shown by the dashed line in Figure 10. The density maximum in the liquid phase can be located with essentially lower accuracy. A fit of Δz_{max} by a logarithmic temperature dependence gives the equation

$$\Delta z_{max}(\sigma) = -5.77 \ln \tau - 3.68, \tag{16}$$

which is also shown in Figure 10.

To clarify the origin of the density maxima in the density profiles and to understand its shift with temperature, we need an analytical expression for the density profile, which accounts for the missing neighbor effect and for the effect of a long-range surface field. Below we derive such an expression for the local density, assuming an exponential density depletion due to the missing neighbor effect as a reference function and taking into account the long-range surface potential as a small perturbation.

The equilibrium density profile should satisfy the following integro-differential equation [2]:

$$\nabla_1 \ln \rho(r_1) + \beta^* \nabla_1 U_w(r_1) = \int dr_2 C^{(2)}(r_1, r_2) \nabla_2 \rho(r_2). \tag{17}$$

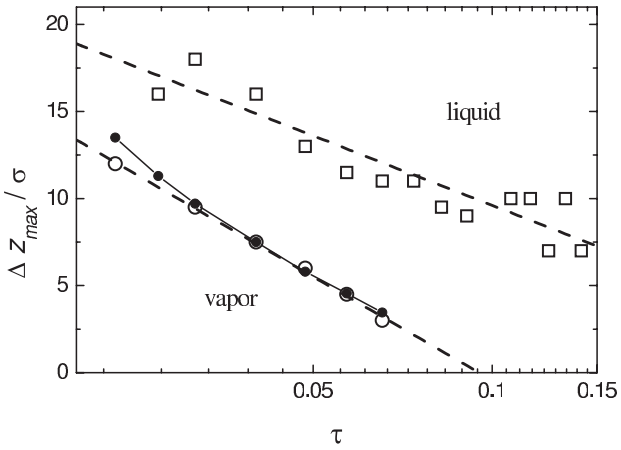

Fig. 10. Location Δz_{max} of the maximum in the density profiles of vapor (open circles) and liquid (open squares) in the pore with $H = 40\sigma$. Equations (15) and (16) are shown by dashed lines. The values Δz_{max} found from equation (26) with $\xi_0 = 0.117\sigma$ are shown by solid circles.

where $C^{(2)}(r_1,r_2)$ is a pair correlation function. In the case of a slowly varying density, which is the case indeed for the studied profiles at $\Delta z > 2\sigma$, the integral on the right side of the equation (17) can be simplified [2]:

$$\int dr_2 C^{(2)}(r_1, r_2) \nabla_2 \rho(r_2) = \nabla_1 \rho(r_1) \int dr_2 C^{(2)}(r_1 - r_2). \tag{18}$$

Near a planar surface the density varies only in the z-direction, normal to the surface. For a weak density gradient we may neglect spatial variations of the pair correlation function. In such a case, equation (17) can be rewritten as:

$$\frac{\partial}{\partial z} \ln \rho(z) + \beta^* \frac{\partial}{\partial z} U_w(z) = \frac{\partial}{\partial z} \rho(z) \int C^{(2)}(r) dr. \tag{19}$$

Using the well-known relation between compressibility χ and pair correlation function $C^{(2)}(r)$ [38], equation (19) reads:

$$\frac{\partial}{\partial z} \ln \rho(z) + \beta^* \frac{\partial}{\partial z} U_w(z) = \frac{\partial}{\partial z} \rho(z) \left(\chi \rho_b / \beta^* - 1\right) / \rho_b. \tag{20}$$

In the absence of a fluid-wall interactions ($U_w(z) = 0$), the density profile $\rho_0(z)$ should satisfy the following equation:

$$\frac{\partial}{\partial z} \ln \rho_0(z) = \frac{\partial}{\partial z} \rho_0(z) \left(\chi \rho_b / \beta^* - 1\right) / \rho_b. \tag{21}$$

Introducing $\Delta\rho(z) = \rho(z) - \rho_0(z)$ as a deviation from the profile in the absence of a fluid-wall interaction, equation (20) becomes:

$$\frac{\partial}{\partial z} \ln \rho(z) + \beta^* \frac{\partial}{\partial z} U_w(z) = \frac{\partial}{\partial z} \rho_0(z) \left(\chi \rho_b / \beta^* - 1\right) / \rho_b + \frac{\partial}{\partial z} \Delta\rho(z) \left(\chi \rho_b / \beta^* - 1\right) / \rho_b. \tag{22}$$

Taking into account equation (21), we obtain:

$$\frac{\partial}{\partial z}\ln\frac{\rho(z)}{\rho_0(z)} = -\beta^*\frac{\partial}{\partial z}U_w + \frac{\partial}{\partial z}\Delta\rho(z)\left(\chi\rho_b/\beta^* - 1\right)/\rho_b. \tag{23}$$

If the perturbation $\Delta\rho(z)$ due to the fluid-wall interaction is small, the second term on the right side of equation (23) may be approximated by the Boltzmann distribution as:

$$\frac{\Delta\rho(z)}{\rho_0(z)} = \exp\left(-\beta^*U_w(z)\right) - 1 \approx -\beta^*U_w(z). \tag{24}$$

Integration of equation (23) yields the following density profile

$$\rho(z) = \rho_0(z)\exp\left[-U_w(z)\rho_b\chi\right]. \tag{25}$$

Near weakly attractive surfaces, the profiles of the saturated liquids and vapors show pronounced density depletion at high temperatures, which originates from the missing neighbor effect [10,11,14] (see also Figs. 8, 9). In this regime, the fluid density profile $\rho_0(z)$, unperturbed by the long-range fluid-wall attraction, follows equation (14) with $\rho_s = 0$ and equation (25) becomes

$$\rho(\Delta z) = \rho_b\left[1 - \exp\left(-\frac{\Delta z}{\xi_-}\right)\right]\exp\left[-U_w(z)\rho_b\chi\right]. \tag{26}$$

This equation reflects two competing surface effects: depletion of the density toward the surface due to the missing neighbors and an opposite trend due to the long-range fluid-wall attraction, that may result in a density maximum.

Equation (26) allows an analysis of the density profile and, in particular, the location of the expected density maximum. For these purposes, we have calculated the isothermal compressibility by equation (12), using the values of the second virial coefficient *B(T)* from Table 1 and third virial coefficient *C(T)* from reference [39]. Note, that contribution of *C(T)* is practically negligible and does not exceed 1% in studied temperature and density range. The values ρ_b of the fluid density far from the wall were taken from Table 1. The values of the dimensionless compressibility $\chi\rho_b/\beta^*$, calculated in such a way, are given in Table 1. We used the asymptotic power law

$$\xi_- = \xi_0\tau^{-\nu} \tag{27}$$

to describe the temperature dependence of the the bulk correlation length in the vapor phase. The amplitude ξ_0 was chosen as 0.117σ in order to reproduce the value ξ_-^{eff} obtained from the fit to exponential equation (14) of density profile at $T = 1.14$, i.e. at the middle of the temperature interval where surface field can be considered as perturbation of strong density depletion near the wall.

The density profiles calculated with equations (26) and (27) are compared with simulation data at $T = 1.11$, 1.12 and 1.13 in Figure 7. Equation (26) gives density maximum rather close to the ones, observed in the simulations. Despite essential underestimation of the amplitude of the density maximum, equation (26) qualitatively reproduces the observed evolution of the density profiles with temperature. In particular, the location of the density maximum, estimated from the simulated density profiles and found from equation (26), well coincide (see Fig. 10 and Tab. 2).

As we can see from Figure 10, the maxima of the density profiles of the saturated liquid are observed further from the surface, in comparison with the saturated vapor at the same temperature. This is directly related to the appearance of a drying layer in the liquid phase near a weakly attractive surface [16]. In the presence of a drying layer the liquid density profile $\rho_0(z)$ can be described by a interfacial-like equation (see Eq. (6) in Ref. [16]). The effect of a fluid-wall potential on such a profile can be considered in a similar way, as described above (see Eq. (25)). Similarly to the vapor case, the values of Δz_{max}, calculated in such a way moves away from the surface with increasing temperature.

4.5 Gibbs adsorption

The temperature evolution of the obtained vapor density profiles reflects a competition of two effects: long-range fluid-wall attraction and the effect of missing neighbors. At low temperatures the wall attraction dominates and yields concave density profiles up to $T \approx 1.10$. At higher temperatures, the missing neighbor effect dominates and the density profiles are convex upwards. This behavior of $\rho_v(\Delta z,\tau)$ is reflected in the temperature dependence of the surface excess adsorption (desorption) Γ. The Gibbs adsorption Γ describes the excess (deficit) of mass per unit surface area and can be calculated from the density profiles:

$$\Gamma = \int_0^{H/2}\rho(\Delta z)d(\Delta z) - \rho_b H/2. \tag{28}$$

The behavior of the density in the first surface layer, where molecules are strongly localized in the minimum of the fluid-wall potential, is quite different from the other layers. Therefore, we analyzed separately the excess adsorption for the first layer, $\Gamma(1\sigma)$, and the adsorption Γ for the rest of the vapor. The values of $\Gamma(1\sigma)$ and Γ, calculated for the pores with $H = 40\sigma$ and $H = 12\sigma$, are shown as a function of the reduced temperature τ in Figure 11.

The excess adsorption in the first layer $\Gamma(1\sigma)$ is positive only at low temperatures, more precisely, in the same range where the density profiles are described by the Boltzmann law for ideal gas (Eq. (9)). When deviations from the ideal gas behavior become noticeable, the deficit of density is observed in the first surface layer. This desorption increases rapidly with increasing temperature and it is clearly related to the missing neighbor effect.

In both pores, a clear crossover of Γ from adsorption regime ($\Gamma > 0$) to depletion regime ($\Gamma < 0$) occurs with increasing temperature (Fig. 11). In the large pore, the crossover temperature, defined as $\Gamma \approx 0$, is about $T = 1.12$, which corresponds to the most 'flat' density

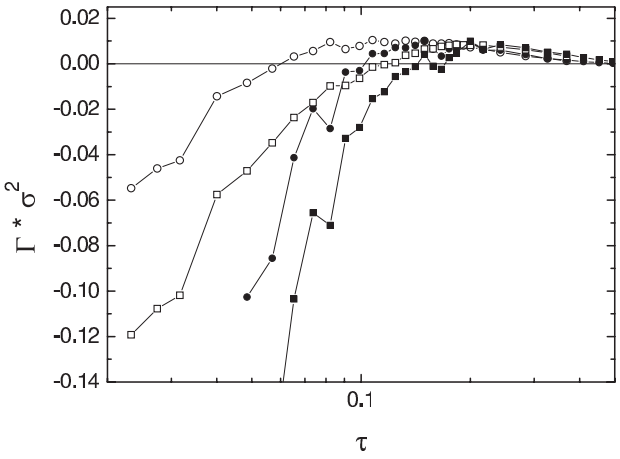

Fig. 11. Gibbs adsorption Γ of the vapor, calculated with equation (28), as function of a reduced temperature τ. Adsorption in the first surface layer $\Delta z \leq 1\sigma$: squares. Adsorption in the range $\Delta z \geq 1\sigma$: circles. Data for the pores with $H = 40\sigma$ and $H = 12\sigma$ are shown with open and solid symbols, respectively.

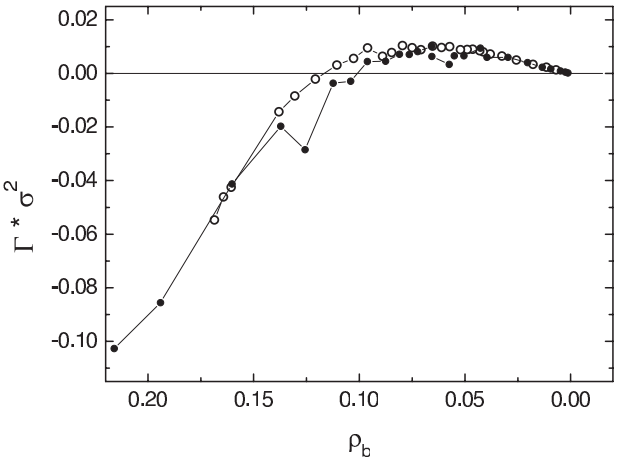

Fig. 12. Gibbs adsorption Γ of the vapor in the range $\Delta z \geq 1\sigma$, calculated with equation (28), as function of the vapor density ρ_b in the pore interior. Data for the pores with $H = 40\sigma$ and $H = 12\sigma$ are shown by open and solid symbols, respectively.

profile at $\Delta z \geq 2\sigma$ which, however, shows a clear maximum (see Fig. 7, middle panel). In the small pore, the crossover temperature from adsorption to depletion is noticeably lower and we estimate it as $T \approx 1.07$. Again, at this temperature the vapor density profile is closest to a horizontal line [10], apart from one to two density oscillations near the wall.

Note, that the behavior of the excess adsorption Γ in the small and large pores becomes almost identical if it is considered as a function of the density in the pore center (Fig. 12). This evidences, that the crossover temperature from adsorption to depletion is determined mainly by the bulk density. For the considered weakly attractive fluid-potential the crossover occurs at $\rho_b \approx 0.12$.

5 Discussion

In computer simulations, the density profiles of a fluid near a wall can be studied only in pore geometry. This results, in general, in a shift of the liquid-vapor phase transition, which diminishes with increasing pore width. To minimize the effect of confinement we used a large slitlike pore of width $H = 40\sigma$. The shift of the liquid-vapor coexistence in the pore can be characterized by the ratio p/p^0 of the saturated vapor pressures in the pore and in the bulk. In ideal gas approximation this ratio is equal to the ratio ρ_b/ρ_b^0, where ρ_b^0 is the density of the saturated bulk vapor. Apart from the three lowest temperatures, the pressure shift remains almost constant at all studied temperatures: $p/p^0 \approx 1.054$, which corresponds to a practically constant shift $\Delta\mu = 0.057$ of the reduced chemical potential. As the latter value is relatively small, we may expect that regularities, obtained for the large pore with $H = 40\sigma$, remain valid for semiinfinite systems.

The analysis of the density profiles reveals several regimes, which are determined mainly by the vapor density ρ_b in the pore interior: (i) ideal gas adsorption; (ii) weak adsorption; (iii) neutral-wall regime; and (iv) strong density depletion. Regime (i) is observed at low temperatures when the bulk vapor density ρ_b does not exceed 0.02 and a second density oscillation near the surface is negligible. The Boltzmann law (Eq. (9)) perfectly describes the density profiles $\rho_v(\Delta z, \tau)$ in this regime. Weak adsorption (ii) is observed when $0.02 < \rho_b < 0.10$, i.e. up to about $T = 1.10$. In this regime the vapor density shows a concave down profile apart from two density oscillations near the surface and this part of the profile can be described by the empirical equation (14) with a surface density ρ_s, exceeding ρ_b. A crossover from adsorption to depletion of vapor is observed in regime (iii), which occurs when ρ_b is about 0.12, when the density profile is roughly flat. Closer to the critical point, in regime (iv), the vapor density is strongly depleted near the wall and can be described by the exponential equation (14) with a surface density $\rho_s < \rho_b$.

Theory of critical phenomena states that intrusion of any short-range surface perturbation into the bulk fluid is governed by the correlation length [17]. Computer simulations of LJ fluid and water confined in small pores with weakly attractive walls evidence a perfect scaling behavior of the order parameter profiles at high temperatures [10,14] and allow estimation of the bulk correlation length. Besides, temperature dependence of the local order parameter indicates, that a crossover from bulk to the surface critical behavior occurs when the distance to the surface is about 2 correlation lengths found from the scaling of the density profiles. Analysis of density profiles in liquid coexistence phase using interfacial equation, which takes into account formation of a drying layer in large pore, yields estimation of the bulk correlation length consistence with ξ_- found in small pores (see Fig. 5 open circles and solid line). The effective correlation length ξ_-^{eff} reported here (Tab. 2) seems to be reasonable in temperature intervals where ρ_v shows strong depletion or strong adsorption (Fig. 5). In the intermediate range, where the

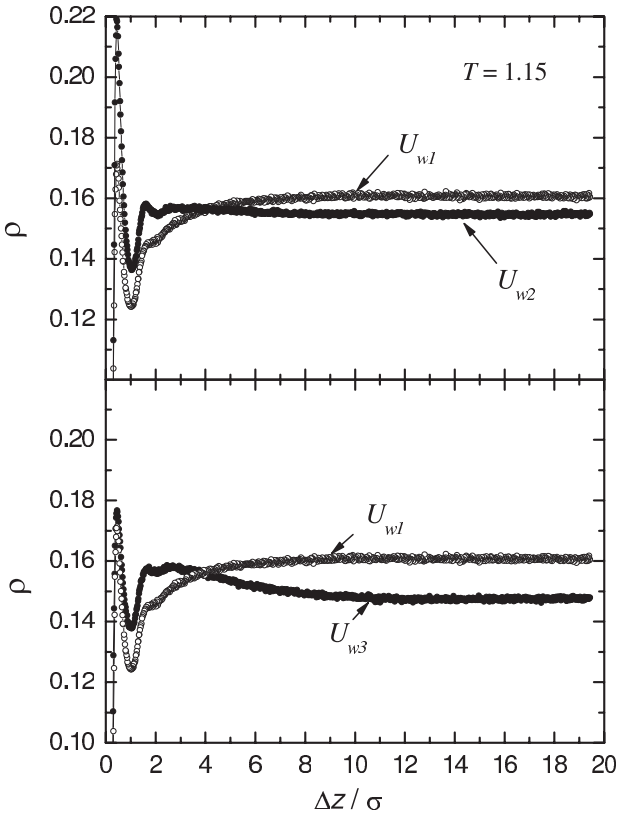

Fig. 13. Density profiles of a saturated LJ vapor at $T = 1.15$ in a pore with $H = 40\sigma$. Enhanced fluid-wall interaction potential $U_{w2}(z)$: upper panel, solid circles. Potential $U_{w3}(z)$ with longer interaction range: lower panel, solid circles. Density profile in a reference system with $U_{w1}(z)$ is shown by open circles.

vapor profile is closed to flat, unreasonable values of ξ_-^{eff} evidences inapplicability of equation (14), when the amplitude of depletion/adsorption is small. Note, that long-range surface-fluid interaction practically does not affect the correlation length determined in liquid phase as far as it was evaluated from the shape of liquid-drying layer interface which is separated from the wall by drying layer, which effectively reduces the effects of the surface.

In regimes (iii) and (iv) a maximum density is observed in the profiles $\rho_v(\Delta z,\tau)$. This maximum separates a concave part in the pore interior and a depleted part near the pore wall and moves away from the surface with increasing temperature. We have shown, that the evolution of this maximum can be described using equation (26), derived from the assumption, that the weak fluid-wall interaction is a small perturbation of the reference system in the absence of a fluid-wall attraction. Contrary to the previous considerations [36,37], a reference, nonperturbed, system was imposed to have an exponential density depletion near the surface. Such profiles are indeed observed close to the critical point in large as well as in small pores. Although, the proposed equation (26) clearly underestimates the amplitude of the maximum, it well reproduces the temperature evolution of the location of the maximum Δz_{max} with respect to the surface.

Vapor density profiles are highly sensitive to the details of the fluid-wall interaction potential. In particular, an increase of the strength of the fluid-wall potential shifts the crossover temperature from adsorption to depletion closer to the critical point. In Figure 13 (upper panel) the vapor density profiles for the pores with fluid-wall potentials U_{w1} and U_{w2} are compared at $T = 1.15$. The regime of density depletion, observed for potential U_{w1}, becomes the regime of a weak adsorption, due to strengthening of a fluid-wall interaction on about 30% for potential U_{w2}. Further strengthening of the fluid-wall interaction should move the crossover temperature to the critical point (an almost flat density profile was observed at the critical point, when the factor f in Eq. (7) is about 0.644 [27]). We also simulated the profile of the coexisting vapor in a pore with fluid-wall interaction potential U_{w3} which possesses the same strength (well-depth) but a larger interaction range than potential U_{w1} (see section Methods for details). The increase of the interaction range affects the vapor density profile in the same way, as its strengthening. At $T = 1.15$ (Fig. 13, lower panel), the regime of density depletion (potential U_{w1}) turns into a regime of a weak adsorption (potential U_{w3}).

We never observed the power-law behavior of density profiles at short distances from the wall, which is observed for magnetization profiles in Ising magnets [17,23,24]. We may assume, that the range of validity of the power-law behavior does not exceed 2σ in the temperature range studied in present paper. Two strong density oscillations dominate in this range and may prevent observation the power-law behavior.

Appearance of the density maximum at Δz_{max} in both coexisting phases may be explained by the interplay of the missing neighbor effect and the *long-range* attractive potential of the pore wall. This idea is strongly supported by the specific temperature evolution of Δz_{max} in both fluid phases: it diverges when approaching the critical temperature. Such behavior is in accord with the absence of this density maximum at $T = T_c$ in the density profiles of LJ fluid near the same wall [27]. The observed maximum has the similar nature as the maximum predicted for the magnetization profiles of the Ising magnets [23,24], which originates from the interplay of the missing neighbor effect and the *short-range* finite surface field. Existence of such maximum of magnetization (density, concentration, etc.) seems to be a general feature of the systems of interacting particles near a boundary with non-zero surface field.

The universal character of the surface critical behavior of fluids may serve as a powerful tool to predict fluid density profiles in various thermodynamic states near various surfaces. Therefore, studies of the surface critical behavior of fluids have both fundamental and practical importance. One of the main problem in this field is a correct mapping of confined fluid onto the much better studied behavior of Ising magnets. Note, however, that even in lattice systems the critical behavior in the presence of a nonzero surface field (the most relevant case for fluids) was studied by simulations in a few papers only [40–43]. In particular, the evolution of the magnetization profiles in *both* coexisting phases was not simulated yet, and the schematic picture, shown in Figure 1, remains to be tested.

Financial support from Deutsche Forschungsgemeinschaft (SPP 1155) is gratefully acknowledged.

References

1. J.D. van der Waals, Z. Phys. Chem. **13**, 657 (1894)
2. R. Evans, Advances in Phys. **28**, 143 (1979)
3. N.B. Wilding, A.D. Bruce, J. Phys.: Condens. Matter **4**, 3087 (1992)
4. R. Steitz, T. Gutberlet, T. Hauss, B. Klosgen, R. Krastev, S. Schemmel, A.C. Simonsen, G.H. Findenegg, Langmuir **19**, 2409 (2003)
5. A.K. Doerr, M. Tolan, T. Seydel, W. Press, Physica B **248**, 263 (1998)
6. A.K. Doerr, M. Tolan, J.-P. Schlomka, W. Press, Europhys. Lett. **52**, 330 (2000)
7. C.-J. Yu, A.G. Richter, A. Datta, M.K. Durbin, P. Dutta, Phys. Rev. Lett. **82**, 2326 (1999)
8. M.E. Fisher, Rep. Progr. Phys. **30**, 615 (1967)
9. H.E. Stanley, *Introduction to Phase Transitions and Critical Phenomena* (Oxford, Clarendon Press, 1971)
10. I. Brovchenko, A. Geiger, A. Oleinikova, Eur. Phys. J. B **44**, 345 (2005)
11. I. Brovchenko, A. Oleinikova, in *Handbook on Theoretical and Computational Nanotechnology*, edited by M. Rieth, W. Schommers (American Scientific Publishers, Stevenson Ranch, CA, 2006), Chap. 62
12. K. Binder, *Phase Transitions and Critical Phenomena*, edited by C. Domb, J.L. Lebowitz (London, Academic Press/London, 1983), Vol. 8, p. 1
13. I. Brovchenko, A. Geiger, A. Oleinikova, Phys. Chem. Chem. Phys. **3**, 1567 (2001)
14. I. Brovchenko, A. Geiger, A. Oleinikova, J. Phys.: Condens. Matter **16**, S5345 (2004)
15. S. Dietrich, in *Phase Transitions and Critical Phenomena*, edited by C. Domb, J.L. Lebowitz (New York, Academic/New York, 1987), Vol. 12, p. 1
16. A. Oleinikova, I. Brovchenko, A. Geiger, J. Phys.: Condens. Matter **17**, 7845 (2005)
17. M.E. Fisher, P.-G. de Gennes, C.R. Acad. Sci. Paris B **287**, 207 (1978)
18. R. Guida, R.J. Zinn-Justin, J. Phys. A: Math. Gen. **31**, 8103 (1998)
19. A. Liu, M.E. Fisher, Phys. Rev. A **40**, 7202 (1989)
20. M. Smock, H.W. Diehl, D.P. Landau, Ber. Bunsenges. Phys. Chem. **98**, 486 (1994)
21. H.W. Diehl, M. Smock, Phys. Rev. B **47**, 5841 (1993)
22. L.V. Mikheev, M.E. Fisher, Phys. Rev. B **49**, 378 (1994)
23. U. Ritschel, P. Czerner, Phys. Rev. Lett. **77**, 3645 (1996)
24. A. Ciach, U. Ritschel, Nucl. Phys. B **489**, 653 (1997)
25. G. Gompper, Z. Phys. B - Condensed Matter **56**, 217 (1984)
26. H.W. Diehl, M. Shpot, Phys. Rev. Lett. **73**, 3431 (1994)
27. A. Maciolek, R. Evans, N.B. Wilding, J. Chem. Phys. **119**, 8663 (2003)
28. J.-L. Barrat, L. Bocquet, Phys. Rev. Lett. **82**, 4671 (1999)
29. B.M. Law, Progr. Surf. Science **66**, 159 (2001)
30. A.Z. Panagiotopoulos, Mol. Phys. **62**, 701 (1987)
31. I. Brovchenko, A. Geiger, A. Oleinikova, J. Chem. Phys. **120**, 1958 (2004)
32. R. Agrawal, D.A. Kofke, Mol. Phys. **85**, 43 (1995)
33. B. Chen, J.I. Siepmann, M.L. Klein, J. Phys. Chem. B. **105**, 9840 (2001)
34. M.A. Barosso, A.L. Ferreira, J. Chem. Phys. **116**, 7145 (2002)
35. N.B. Wilding, Phys. Rev. E **52**, 602 (1995)
36. W.A. Steel, *The interaction of gases with solid surfaces* (Pergamon Press, Oxford, 1974), p. 349
37. G.H. Findenegg, J. Fischer, Faraday Disc. **59**, 38 (1975)
38. J.-P. Hansen, I.R. McDonald, *Theory of simple liquids* (Academic Press, London, 1986), p. 556
39. J.O. Hirschfelder, C.F. Curtiss, R.B. Bird, *Molecular theory of gases and liquids* (John Wiley, New York, 1964), p. 1249
40. K. Binder, D.P. Landau, Phys. Rev. B **37**, 1745 (1988)
41. K. Binder, D.P. Landau, S. Wansleben, Phys. Rev. B **40**, 6971 (1989)
42. K. Binder, D.P. Landau, J. Chem. Phys. **96**, 1444 (1992)
43. K. Binder, A.M. Ferrenberg, D.P. Landau, Ber. Bunsenges. Phys. Chem. **98**, 340 (1994)